

The Effect of finite strain and deformation history of HALABAN area, eastern Arabian shield, Saudi Arabia

Yousef A. Al-Amri¹ · Osama M. K. Kassem^{1,2}

Received: 6 October 2016 / Accepted: 26 December 2016 / Published online: 7 January 2017
© Saudi Society for Geosciences 2017

Abstract The present study aims to evaluate a relationship between the mineralogy and structural analysis in the Halaban area and to document the tectonic evolution of Halaban and Al Amar faults. The collected samples were taken from deformed granitoids rocks (such as granite, gneisses and tonalite), metasedimentary, metavolcanic, metagabbro and carbonate rocks are trend to NE-SW with low dip angle in the Halaban area. These samples were 8 from granite, 14 metagabbro, 6 metavolcanics, 5 tonalite, 6 metasedimentary, 10 gneisses and 8 carbonate rocks. Our results are described for the different axial ratios of deformed rocks as the following: XZ sections range from 1.10 to 4.60 in the Fry method and range from 1.70 to 2.71 in the Rf/φ method. YZ sections range from 1.10 to 3.34 in the Fry method and range from 1.62 to 2.63 in the Rf/Phi method. In addition, XY sections range from 1 to 3.51 in the Fry method and range from 1 to 1.27 in the Rf/φ method for deformed granite rocks, metasedimentary rocks, and metagabbro. The stretch axes for measured samples in the X direction axes (S_X) variety from 1.06 to 2.53 in the Fry method and vary from 1.20 to 1.45 in the Rf/φ method. The values of the Y direction axes (S_Y) vary from 0.72 to 1.43 in the Fry method, which indicates contraction and extension in this direction and vary from 1.13 to 1.37 in the Rf/φ method which indicates extension in this direction. Furthermore, the Z

direction axes (SZ) varies from 0.09 to 0.89 in the Fry method and from 0.52 to 0.71 in the Rf/φ method. The stretches axes in the Z direction (SZ) show a vertical shortening about 11% to 91% in the Fry method and show vertical shortening about 29% to 48% in the Rf/φ method. The studied rock units are generally affected by brittle-ductile shear zones, which are sub-parallel to parallel NW or NNW trend. It assumed that different rock types of have similar deformation behavior. Based on these results, it is concluded that the finite strain is accumulated during the metamorphism after that was started the deformation by thrusting activity. The contacts between the different rock types were deformed during thrusting under semi-brittle to ductile deformation conditions by simple shear. A component of vertical shortening is also involved causing subhorizontal foliation in the Halaban area.

Keywords Finite strain · Deformation · Halaban area · Arabian shield · Saudi Arabia

Introduction

Many authors investigated the geology and geochemistry of the Halaban area (e.g. Stoeser, 1986; Al-Saleh et al., 1998; Al-Saleh and Boyle, 2001). The Halaban Ophiolite Belt is the biggest ophiolite sheets in the Arabian Shield. Many authors explained the structural analysis of the deformed lithologies exposed in the Halaban area in the east of the Arabian Shield (Fig. 1). Rocks to the east are low-grade metasedimentary units of the Abt Formation and post-amalgamation granitoids. The ophiolitic rocks crop out in hills with relief of about 50 m and are generally well exposed. Unfortunately, the margins of the ophiolite tend to coincide with valleys so that structural details at the boundaries of the ophiolite are largely obscured. From

✉ Yousef A. Al-Amri
yaalamri@ksu.edu.sa

Osama M. K. Kassem
kassmol@yahoo.com

¹ SGSRC, Department of Geology, Science faculty, King Saud University, P.O. Box 2455, Riyadh 11451, Kingdom of Saudi Arabia

² Department of Geology, National Research Center, Al-Behooth str, Dokki, Cairo 12622, Egypt

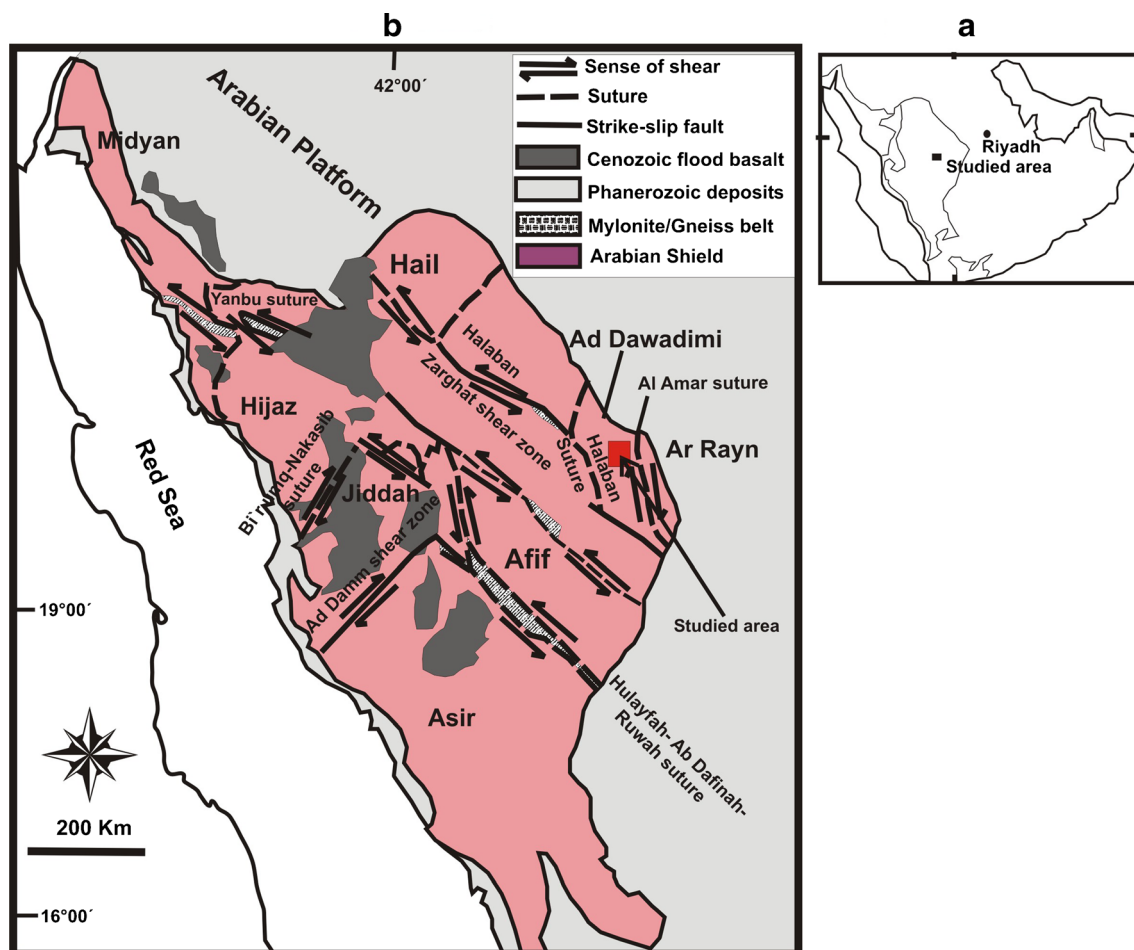


Fig. 1 a) Location of studied area. b) Tectonostratigraphic terranes in the Arabian Shield (After Nehlig et al., 2002)

the point of view of the Penrose definition, the rocks in the vicinity of Halaban do not include mantle peridotite, a dike complex, or pillow basalt and, at best, are an incomplete ophiolite (Johnson et al., 2011). However, the on-strike continuation of the Halaban rocks includes peridotite, gabbro, serpentinite, listwaenite, and basalt (Al-Shanti and El-Mahdy, 1988). It is possible that the rocks in the vicinity of Halaban village are the mafic plutonic section of an ophiolite, whereas the mantle part is preserved in the north (Fig. 2).

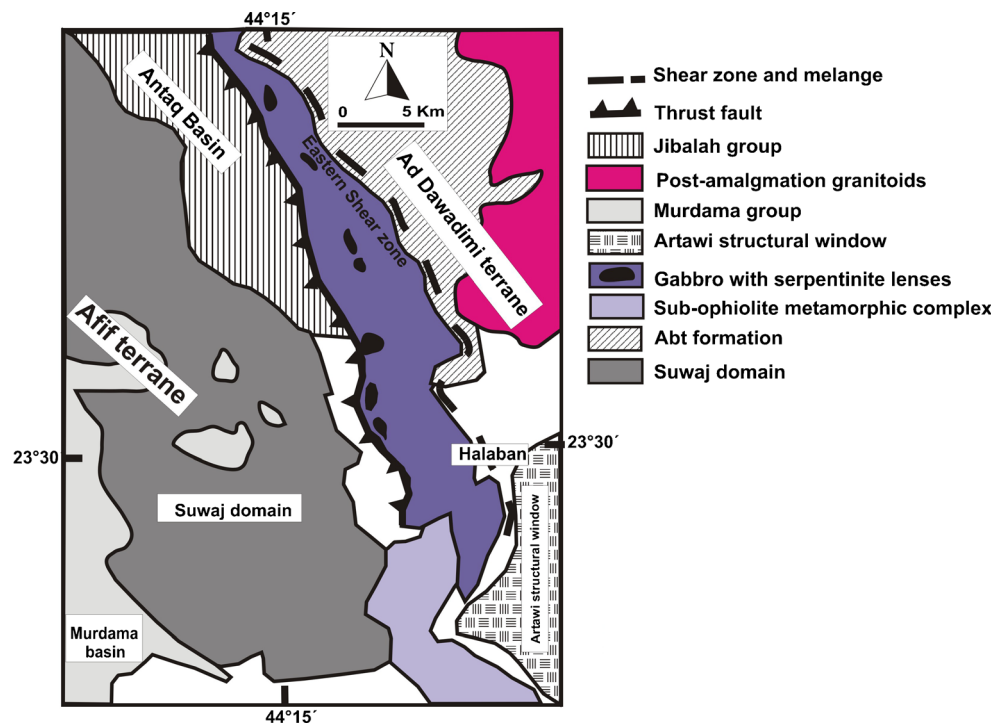
Structural technique on the deformed lithologies was explained in the Halaban area in the east of the Arabian Shield. This work was achieved through field work, microstructural and petrology investigation to quantify the finite strain in the Halaban area, felsic and mafic grains have been analyzed by the R_f/ϕ and fry methods (Ramsay and Huber, 1983). It used three finite strain axes such as XY, XZ and YZ sections ($X \geq Y \geq Z$) to estimate the three dimensional strain geometry. The R_f/ϕ describe the fabric ellipsoid or clast strain and determined Finite strains for measured samples (Ramsay and Huber 1983;

Kassem and Ring 2004; Kassem and Abdel Raheim, 2010; Kassem, 2011, 2014, 2015; Kassem et al., 2012; Al-Saleh and Kassem, 2012; Kassem and Hamimi, 2014).

Many authors suggested that the Arabian Shield may be the result of a fusion of a number of arcs islands that originated in the ocean basin above the oceanic crust and put the models for that (e.g. Al-Shanti and Mitchell, 1976; Gass 1977; Schmidt et al., 1979 and Camp, 1984). On the other hand, some authors (Garson and Shalaby, 1976; Delfour, 1981 and Kemp et al., 1982) believed that the Arabian Shield has originated and the evolution of either the formation tectonic of activity melting or fission of the continental crust of siliciferous earthbound old or a combination of both. This application can the theory of the composition Arabian Shield a fusion a number of island arcs and theory is prevalent and acceptable.

In the present work, we aims to study and declare the structural history and the geometry of the Halaban area through some information about finite strain, strain variation patterns and deformation history for collected

Fig. 2 Simplified map of the Halaban ophiolite complex and adjacent units (Al-Saleh et al., 1998)



samples from Halaban area. In the concerned area, we use these data from finite strain and the behavior of the tectonic contact during deformation.

Geological Background

The Arabian Shield structurally related to the diverse and polyphase geodynamic events (Fig. 1). The Arabian Shield be the result of a fusion a number of small plates, and this theory shows the distribution of the five different geological regions in the Arabian Shield, which separates it from each other by Sutures a fusion tectonic exposed to it belts ophiolite are clear (e.g. Vail, 1983; Camp, 1984 and Stoesser et al., 1984; Al-Shanti and Abo Omar, 2003). Stoesser and Camp (1985) divided of the Arabian Shield to five regions of geologically and tectonically, two regions Afif and Al Rayn region which is most likely that is continental origin, which represent the eastern part of the Arabian Shield. Either the other three regions are Asir and the Hijaz and the Madyan of which consisting of arcs Islands within the oceanic crust, which represent the western part of the Arabian Shield (Fig. 1). Recently, Doebrich et al. (2007) suggested that the geological map of the Arabian Shield divided into eight regions, Asir region, Jiddah region, Hijaz region and Madyan region, which represented the western part of the shield, while Afif region, Dawadimi region, Hail region and Ar Rayn region represent the eastern part of the Arabian shield (see Fig. 1). Doebrich et al. (2007) suggested that geological map of the Arabian

Shield are shown six intermittent belts of mafic and ultramafic rocks and which separates to eight regions of the Arabian Shield and parallel to the appears general extensions for groups of layered rocks. Halaban belt separated Afif and Ad Dawadimi regions which represented by the tectonic movement (Doebrich et al., 2007).

The geological setting for studied area is characterized by two main stratigraphic units: ophiolite complexes and Abt Formation clastic sediments, which represent the Urd Group (Delfour, 1979). The Urd Group is thought to form a broad synclinorium with the ophiolitic rocks at the base and the Abt Formations the core (Delfour, 1979). The ophiolitic rocks are composed mainly of serpentinitized harzburgite, dunite, gabbro, and tholeiitic metabasalt in which pillow structures are locally preserved. Chert and ferruginous jasper are intercalated with the metabasalt (Delfour, 1979). Siliceous calc-dolomite rock (listwaenite) occurs throughout the belts (Fig. 2). The Halaban Ophiolite Belt is replaced by a heterogeneous assemblage of metabasites, metasediments and serpentinites that make up the sub-ophiolitic metamorphic complex (Al-Saleh and Boyle, 2001). Due east of this complex is an area of low relief underlain mainly by heterogeneous granitic rocks of the Abu Isnun Pluton associated with the high-grade schists and migmatites of the Artawi structural window (Fig. 2). Along the eastern margin of the Afif Terrane and west of the Halaban Gabbro Belt is the southern extension of the Suwaj talc-alkaline magmatic arc (Stoesser, 1986). A biotite monzogranite from the Abu Isnun pluton was investigated by Delfour (1979). He interpreted this complex to be of

Middle Proterozoic age or older, but stratigraphically above the older basement unit, and intrusive into the Urd group. It is considered that this monzogranite is primarily a product of partial melting of the Abt Formation and that it inherited zircons from that source, or perhaps from the older Afif crust. In any case, some authors do not accept it as an older basement plutonic unit, but rather as a younger syntectonic intrusive rock, similar in age to the others intruding the Urd group (Fig. 2).

The Abt Formation, or Abt schist, is a folded monotonous series of sericite and/or chlorite schist occupying a belt approximately 40 km wide between the Urd mafic belt at Halaban and the Al Amar fault (Delfour, 1979, 1981). The unit consists of sericite-chlorite schist that grade to lightly metamorphosed fine-grained greywacke and subordinate carbonaceous schist, conglomerate, arkosic sandstone, and dolomitic marble (Delfour, 1979). The unit is generally metamorphosed to the upper green schist facies, but near intrusions may reach the amphibolite facies. The Abt Formation is predominantly thin bedded and tightly to isoclinally folded, with ubiquitous shears nearly parallel to bedding planes. Schistosity is generally parallel to bedding plane except in fold closures and is commonly crenulated by refolding.

Sampling and data Collection

A total of 57 samples were collected from Halaban area. It is found west of Riyadh region on the road to Mecca, Riyadh and about 300 km in high away from Riyadh city. Halaban area located between latitudes N 23° 22' and N 23° 33' and longitudes E 044° 11' and E 44° 25' (Fig. 3). The collected samples are represented the different rock types such as granitoids, metagabbro, Metavolcano-sedimentary rocks, gneisses, and schist.

In the present area, we used to quantify the finite strain for deformed granite, metavolcanic and metasedimentary in the Halaban area such as feldspar (K-feldspars and plagioclase) grains, quartz and mafic grains (hornblende, biotite and chlorite) have been measured by two techniques such as R_f/ϕ and Fry methods (Fry 1979; Ramsay 1967; Ramsay & Huber 1983). We are treated plagioclase and K-feldspar together, because the deformation behavior of them is rather similar. In other case, Passchier and Trouw 1995 suggested that the deformation behavior of mafic minerals such as mica and amphibolites minerals deformed only by slip and twinning and slip. Also, the hardness of silicate minerals are more than some mafic minerals. Therefore, we analyzed the silicate minerals separately from mafic minerals to show the difference between them. For using two methods, the Fry strains are thought to represent the matrix strain, whereas the strain derived from R_f/ϕ technique describe the fabric ellipsoid or clast strain (Ramsay & Huber 1983; Ring 1998).

Deformation INVESTIGATION

In this work, using the thin sections to investigate the finite strain and microstructural analysis. The collected samples cut in two direction; the lineation (XZ) and normal to the foliation and lineation (YZ) to study the thin sections. The direction of lineation for measured samples trend to SE-NW with low to moderate plunging and characterized by mineral lineation and elongated fabric. The foliation direction for deformed rocks as granitoids (such as granite, gneisses and tonalite), metasedimentary, metavolcanic and metagabbro rocks are trend to northeast - southwest with low dip in the Halaban area.

The collected samples in the field work represent the deformed granitoids for all type of rocks such as granite, gneiss and tonalite. Granite is composed mainly of K-feldspar, plagioclase, quartz, hornblende amphibole, and biotite. Accessory minerals are apatite, zircon and chlorite. Granite are sometimes represented by elongated potash feldspars grains and rotated plagioclase and quartz with low to moderate deformation (Fig. 4a). Gneisses consists of quartz, alkali-feldspar (orthoclase), plagioclase and some mafic minerals (biotite and hornblende). In the present work, gneisses show the moderately to highly deformed grains (Fig. 4b). Tonalite includes quartz, alkali-feldspar (orthoclase), plagioclase, and biotite. It is characterized by weakly to moderate deformed (Fig. 4c). The metasedimentary samples are low to moderately deformation, which consists of quartz, elongated hornblende and chlorite. They are called as hornblende-chlorite -quartz schist (Fig. 4d). They are characterized by rotated quartz, elongated hornblende and chlorite (Fig. 4d).

Deformed metagabbro rocks contain plagioclase, hornblende and clinopyroxene. Sometimes metagabbros displayed as elongated plagioclase grains with low to moderate deformation (Fig. 4e). In the present work, two types of metagabbroic rocks are documented in the studied area: layered metagabbro and massive metagabbro. Layered metagabbro is shown plagioclase and pyroxene rich as layers. The pyroxene mineral are characterized by complete to partial altered to secondary type for amphibole and chlorite. Petrographic studies show that the primary and secondary textures for igneous rocks are displayed in the layered metagabbro. The igneous textures involved of plagioclase and shows undulose extinction (Fig. 4e).

The serpentinites rocks constitute masses within the studied area (Fig. 4f). The serpentinites rocks along beside thrust faults and shear zones. They are characterized by fine grain and pale brown, buff to light creamy color. The serpentinites are contained of talc, antigorite,

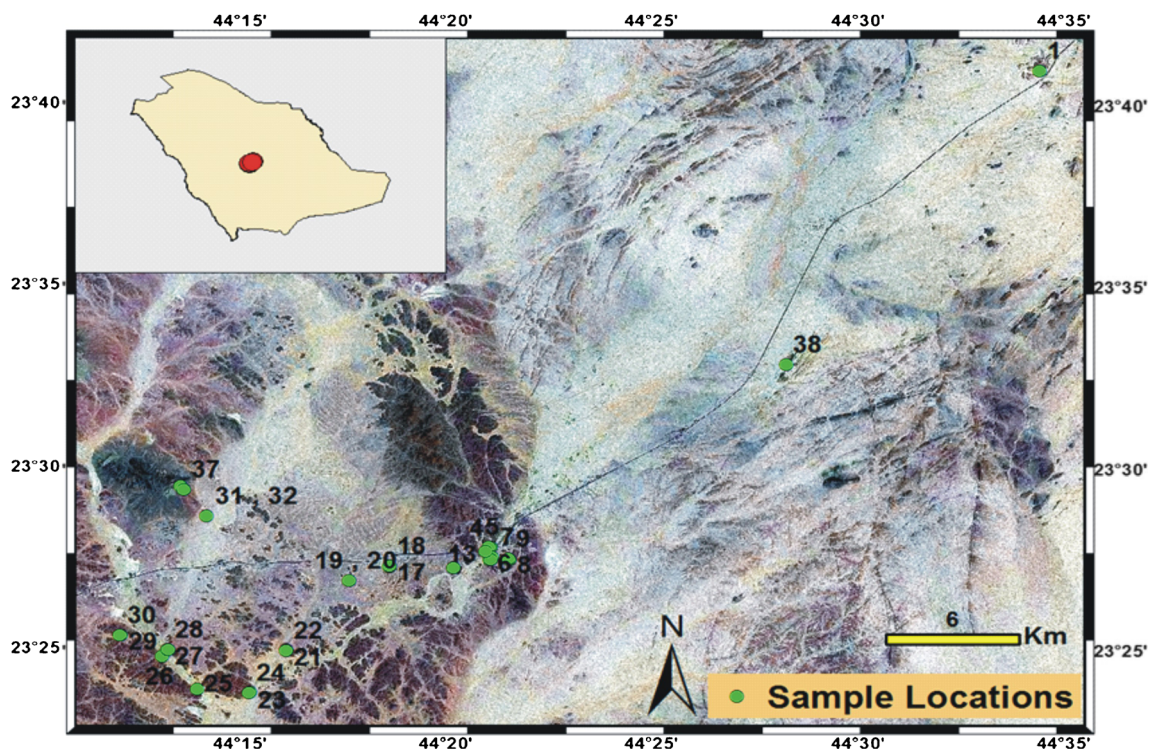


Fig. 3 Landsat map showing samples locations in the Halabian area

and ankerite and accessories minerals such as magnetite and chromite (Fig. 4f). The carbonate rock is contained of calcite, which sometimes is rotated. The carbonate rocks have low deformation (Fig. 4g).

The metavolcanic rocks are represented by meta-diabase and meta-andesite rocks, which consist of plagioclase and hornblende. These minerals as phenocrysts embedded in groundmass in this section. Quartz crystals also displayed as seriate texture (Fig. 4h). The volcanic rocks (meta-rhyolite) are characterized by moderate to high deformed and consist of k-feldspars, quartz and plagioclase. Plagioclase phenocrysts, muscovite and biotite are elongated and sometimes plagioclase is rotated. Elongated quartz crystals have the same orientation as muscovite fishes (Fig. 4h).

It is observed that Rootless intrafolial folds and low-angle discordances between the planes of gneissosity are shown in Fig. 5a. This strongly foliation could be related to the first deformational event, which led to a metamorphic banding and may be synchronous with the alternating bands of biotite- and hornblende gneisses under amphibolite facies condition. Also, the different type rocks in the studied area show distinct centimeter- to decimeter-thick lithological banding parallel to the gneissosity (Fig. 5b). This banding dominates the outcrop in many places and is interpreted to be related to stretching of mixed igneous lithologies (e.g. xenoliths, enclaves, mafic and felsic dykes, sills, etc.) by intense strain.

Results of finite-strain analysis

Finite strain axial ratios

Our results for Fry and R_f/ϕ methods are described for the different axial ratios as the following: XZ sections range from 1.10 to 4.60 in the fry method and 1.70 to 2.71 in the R_f/ϕ method for deformed granitoids rocks, metavolcano-sedimentary rocks, and metagabbros (Table 1). YZ sections range from 1.10 to 3.34 in the fry method and 1.62 to 2.63 in the R_f/ϕ method for all type of rocks (Table 1). In addition, XY sections range from 1 to 3.51 in the fry method and 1 to 1.27 in the R_f/ϕ method for different type of rocks (Table 1).

The stretches axes for measured samples in the studied area are presented in Table 1. The X direction axes (S_x) variety from 1.06 to 2.53 in the fry method and 1.20 to 1.45 in the R_f/ϕ method for deformed granitoids, metavolcano-sedimentary, and metagabbros rocks (Table 1). The Y direction axes (S_y) variety from 0.72 to 1.43 in the fry method and 1.13 to 1.37 in the R_f/ϕ method for deformed rocks, which indicates contraction and extension in this direction (Table 1). Furthermore, the Z direction axes (S_z) variety from 0.09 to 0.89 in the fry method and 0.52 to 0.71 in the R_f/ϕ method for different deformed rocks (Table 1). The stretches axes in the Z direction (S_z) show vertical shortening about 11% to 91% in the fry method and about 29% to 48% in the R_f/ϕ method.

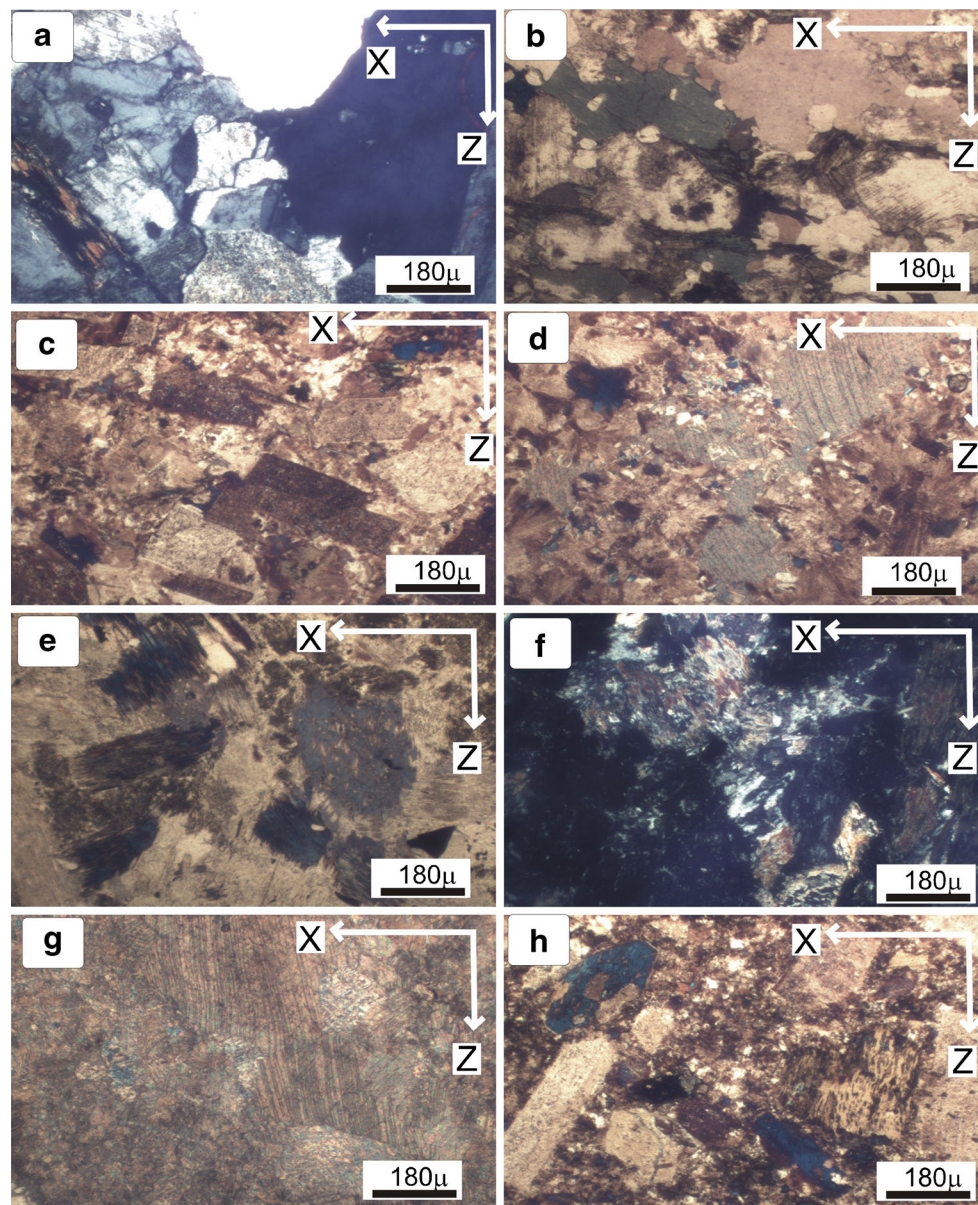


Fig. 4 Photomicrographs of (a) Granite consist of K feldspars, plagioclase and biotite hornblende with moderately deformed (Sample No. Hb1). (b) Migmatized tonalite gneiss include quartz, alkali-feldspar, plagioclase biotite and hornblende (Sample No. Hb17). (c) Granophytic tonalite consist of quartz, alkali-feldspar (orthoclase), plagioclase, and biotite with weakly to moderate deformed (Sample No. Hb 26). (d) Metasedimentary consist of quartz, elongated hornblende and chlorite

(Sample No. Hb 37). (e) Foliated metagabbro contain plagioclase, hornblende and clinopyroxene (Sample No. Hb4). (f) Carbonatized serpentinitized contained of talc, antigorite, and ankerite and accessories minerals (Sample No. Hb 16). (g) Carbonate rocks contained of calcite with low deformation (Sample No. Hb 35). (h) Deformed metavolcanic rocks represented by meta-d diabase and meta-andesite rocks, which consist of plagioclase and hornblende (Sample No. Hb 31)

Strain symmetry

The strain symmetry is explained by Flinn 1962 and Ramsay & Huber 1983, which characterized the strain symmetry by the K value. The K value is ranged from 0.01 to 8.65 and 0.01 to 0.30 in the axial ratios for deformed granitoids, metavolcano-sedimentary succession, and metagabbros rocks by using the fry and Rf/ϕ methods respectively (Table 1). The Nadi strain sections variety from 0.07 to 1.15 in the fry method and 0.42 to 0.80 in the Rf/ϕ method in the axial ratios of

method for different collected samples (Table 1). In addition, the Lode's parameters range from -0.76 to 0.99 in the Fry method and 0.45 to 0.99 in the Rf/ϕ method for deformed rocks (Table 1).

Magnitudes of finite strain

The finite strain data are summarized in a Flinn plot (see Fig. 6 and Table 1). Flinn plot shows the relationship between the relative shapes for strain ellipsoid. Many authors divided the

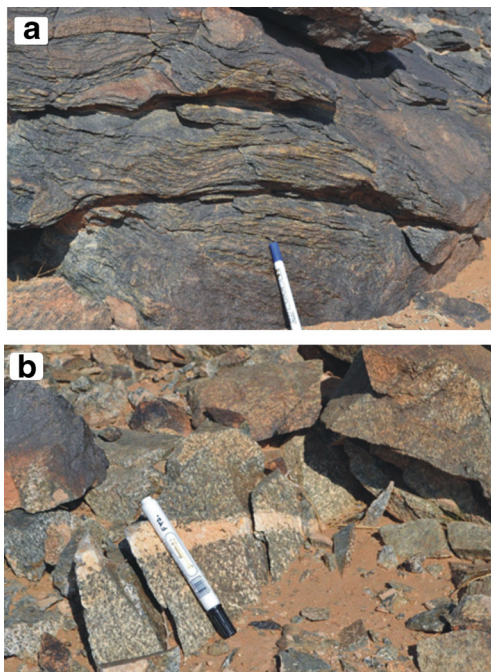


Fig. 5 Field photographs showing (a) the gneissosity with the occasional rootless intrafolial folds. (b) Quartzite bands and lenses are interbedded with foliation in the Metavolcano-sedimentary rocks

strain symmetry into prolate vs oblate ellipsoids shape (Hossack 1968), that represented the constructional vs flattening for strain type. In addition, the volume of strain is important. However, in the basement rocks porosities are very small specially in high grade deformed rocks. Minor or no volume changes are expected for basement rocks during deformation (Kassem & Ring 2004).

The Fry strains show two types of ellipsoids flattening and constructional symmetry (Fig. 6). The flattening type is the majority samples for the Fry technique. Some samples show constructional symmetry. Hence, the measured sample for the fry method derived from measurements of quartz, alkali-feldspar, plagioclase and some mafic minerals. The majority of ellipsoids have oblate field strain symmetry and some data points in the prolate field for the fry method (Fig. 6).

The R_f/ϕ method indicates the flattening symmetry for all measured samples such as deformed granitoids rocks, metavolcano-sedimentary rocks, and metagabbros. In this case, the all measured ellipsoids have oblate field strain symmetry for R_f/ϕ method (Fig. 6). The ratio between XZ vs YZ shows positive correlation (Fig. 7a). The ratio for XY increases with XZ and shows straight correlation (Fig. 7b).

Our strain data explains that the relationship between the tectonic nappe and the strain magnitude does not show in the Halaban area. The average magnitude of strain in the deformed granitoids, metasedimentary, and metagabbro rocks is in a range from 0.07 to 1.15 for Fry method and 0.42 to 0.80 for R_f/ϕ method, which show a very low heterogeneous deformation (Table 1). The measured samples for R_f/ϕ data are

less than Fry data for the relationship between strain magnitude (ET) vs strain symmetry (K). Also the relationship between K vs (ET) shows pronounced straight correlation (Fig. 8a). In addition, the ratio between Lode's parameter (LP) vs strain symmetry (K) indicates that the R_f/ϕ data less than Fry data. The axial ratio between K vs LP shows pronounced negative correlation (Fig. 8b). In other case, R_f/ϕ and Fry methods show mainly constant for the relationship between Strain magnitude (ET) vs Lode's parameter (LP) (Fig. 8c).

The stencches X axis (SX) vs strain symmetry (K) shows a positive correlation (Fig. 9a). Furthermore, the stencches Y axis (SY) vs strain symmetry (K) indicates a negative correlation (Fig. 9b). Also, the stencches Y axis (SY) vs strain symmetry (K) shows a no obvious correlation (Fig. 9c).

Discussion

The Halaban suture, the join between Ad Dawadimi and east of Afif terrane, is represented by a linear belt of ophiolite (the Halaban ophiolite) along the southern part of the Halaban-Zarghat fault and by a metamorphic sole-complex beneath the ophiolite. The metamorphic age of the sole-complex indicates that the Ad Dawadimi and Afif terranes were in place by 680 Ma.

The At Amar suture between the Ad Dawadimi and Ar Rayn terranes is a high-angle fault zone (the Al Amar fault) associated with narrow lenses of carbonate altered ultramafic rock. The suture coincides with a prominent magnetic and gravity gradient. Geologic mapping suggests that the Al Amar fault is vertical to steeply dipping. This variation in fault-plane attitude is consistent with proposals that the region west of the Al Amar fault and may be part of a zone of imbricate listric structures. Convergence of the Ad Dawadimi and At Rayn terranes is not well dated but is constrained to be between 670 and 640 Ma by the age of syn- and posttectonic plutons in the Ar Rayn terrane.

These suturing events are part of the main period of crustal accretion in the Arabian shield. This period, ranging from about 680 Ma to 640 Ma, included suturing between the Afif terrane and the Asir-Jiddah-Hijaz terranes. It also is elongate north-south parallel to the Nabitah fault in the eastern part of the Asir terranes, and at places in the Ar Rayn terrane. Named after the Nabitah fault, this period of accretion is referred to as the Nabitah orogeny. It reflects the virtual completion of assembly of the Arabian shield coincident with the terminal phase of convergence between East and West Gondwana.

The first phase of folding was synmetamorphic and is mostly expressed at outcrop by a chlorite-sericite foliation (S1) concordant to the bedding (Su) along the limbs of the folds. Exudation lenses of quartz, chlorite and calcite

Table 1 Finite strain data for samples from Halaban area

Sample No.	Method	Rxy	Ryz	Rzx	Stretch			Principal strain Ratios K	Strain magnitude Et	lode's parameter	
					Sx	Sy	Sz				
Hb1	1Hb1	Rf/PHI	1.07	1.98	2.12	1.31	1.23	0.62	0.07	0.59	0.82
	1Hb1	Fry	1.13	3.34	3.79	1.63	1.43	0.43	0.06	1.04	0.81
	5Hb1	Rf/PHI	1.17	1.96	2.29	1.39	1.19	0.61	0.18	0.62	0.62
	5Hb1	Fry	1.02	1.65	1.69	1.2	1.17	0.71	0.04	0.42	0.91
Hb3	1Hb3	Rf/PHI	1.02	1.87	1.9	1.25	1.22	0.65	0.02	0.52	0.95
	1Hb3	Fry	2.8	1.37	3.84	2.21	0.79	0.57	4.87	1.00	-0.53
	5Hb3	Rf/PHI	1.05	1.74	1.83	1.25	1.18	0.68	0.07	0.48	0.83
	5Hb3	Fry	1.95	1.58	3.09	1.82	0.93	0.59	1.64	0.80	0.19
Hb4	1Hb4	Rf/PHI	1.12	1.87	2.1	1.33	1.19	0.63	0.14	0.56	0.69
	1Hb4	Fry	1.23	1.61	1.97	1.34	1.09	0.68	0.38	0.49	0.40
	5Hb4	Rf/PHI	1.04	2.47	2.56	1.39	1.34	0.54	0.03	0.75	0.92
	5Hb4	Fry	1.44	1.94	2.8	1.59	1.1	0.57	0.47	0.74	0.29
Hb6	1Hb6	Rf/PHI	1.06	2	2.11	1.31	1.24	0.62	0.06	0.59	0.86
	1Hb6	Fry	1.10	1.93	2.12	1.33	1.21	0.63	0.11	0.58	0.75
	2Hb6	Rf/PHI	1.13	1.87	2.10	1.33	1.18	0.63	0.15	0.56	0.68
	2Hb6	Fry	1.26	2.34	2.94	1.55	1.23	0.53	0.19	0.80	0.58
Hb7	1Hb7	Rf/PHI	1.16	1.98	2.30	1.39	1.19	0.60	0.17	0.63	0.64
	1Hb7	Fry	1.41	1.76	2.48	1.52	1.08	0.61	0.53	0.65	0.25
	3Hb7	Rf/PHI	1.03	1.85	1.90	1.25	1.21	0.66	0.04	0.51	0.90
	3Hb7	Fry	1.63	1.60	2.60	1.62	0.99	0.62	1.04	0.68	-0.02
Hb8	4Hb7	Rf/PHI	1.09	1.93	2.11	1.32	1.21	0.63	0.10	0.58	0.76
	4Hb7	Fry	1.00	1.84	1.85	1.23	1.22	0.66	0.01	0.50	0.99
	1Hb8	Rf/PHI	1.06	1.93	2.05	1.30	1.22	0.63	0.07	0.56	0.83
	1Hb8	Fry	1.30	2.18	2.82	1.54	1.19	0.55	0.25	0.76	0.50
Hb9	5Hb8	Rf/PHI	1.13	2.08	2.35	1.39	1.22	0.59	0.12	0.65	0.71
	5Hb8	Fry	1.52	1.22	1.86	1.42	0.93	0.76	2.37	0.45	-0.36
	2Hb9	Rf/PHI	1.06	2.08	2.20	1.33	1.25	0.60	0.05	0.62	0.86
	2Hb9	Fry	1.20	1.30	1.56	1.23	1.03	0.79	0.65	0.31	0.19
Hb10	5Hb9	Rf/PHI	1.05	2.06	2.17	1.32	1.25	0.61	0.05	0.61	0.87
	5Hb9	Fry	1.54	1.40	2.15	1.49	0.97	0.69	1.34	0.54	-0.12
	1Hb10	Rf/PHI	1.11	1.93	2.14	1.33	1.20	0.62	0.12	0.58	0.73
	1Hb10	Fry	1.32	1.53	2.02	1.39	1.05	0.69	0.59	0.50	0.22
Hb12	4Hb10	Rf/PHI	1.05	2.10	2.21	1.32	1.26	0.60	0.05	0.63	0.87
	4Hb10	Fry	1.42	1.33	1.89	1.39	0.98	0.74	1.28	0.45	-0.10
	12Hb2	Rf/PHI	1.07	2.10	2.25	1.34	1.25	0.60	0.06	0.64	0.83
	12Hb2	Fry	2.52	1.16	2.92	1.95	0.77	0.67	9.50	0.82	-0.72
Hb14	12Hb3	Rf/PHI	1.18	2.20	2.60	1.45	1.23	0.56	0.15	0.72	0.65
	12Hb3	Fry	1.11	1.17	1.30	1.13	1.02	0.09	0.67	0.19	0.19
	14Hb4	Rf/PHI	1.27	1.89	2.40	1.45	1.14	0.60	0.30	0.64	0.45
	14Hb4	Fry	1.74	1.33	2.32	1.59	0.91	0.69	2.24	0.61	-0.32
Hb16	14Hb5	Rf/PHI	1.04	2.25	2.35	1.35	1.29	0.57	0.04	0.68	0.90
	14Hb5	Fry	1.44	1.61	2.31	1.49	1.04	0.65	0.71	0.59	0.14
	16Hb1	Rf/PHI	1.03	2.63	2.71	1.41	1.37	0.52	0.02	0.80	0.94
	16Hb1	Fry	1.00	1.51	1.51	1.15	1.14	0.76	0.01	0.34	0.98
Hb17	17Hb1	Rf/PHI	1.03	2.04	2.10	1.29	1.25	0.62	0.03	0.59	0.92
	17Hb1	Fry	1.31	1.30	1.70	1.31	1.00	0.77	1.03	0.38	-0.01
	17Hb5	Rf/PHI	1.04	1.94	2.02	1.28	1.23	0.63	0.04	0.56	0.89
	17Hb5	Fry	1.18	1.10	1.30	1.15	0.98	0.89	1.82	0.19	-0.27
Hb18	18Hb1	Rf/PHI	1.05	2.00	2.10	1.30	1.24	0.62	0.05	0.59	0.87
	18Hb1	Fry	2.75	1.15	3.16	2.06	0.75	0.65	11.65	0.88	-0.76
	18Hb2	Rf/PHI	1.10	2.00	2.20	1.34	1.22	0.61	0.10	0.61	0.75
	18Hb2	Fry	1.67	1.41	2.35	1.58	0.95	0.67	1.63	0.61	-0.20
Hb19	18Hb4	Rf/PHI	1.05	2.10	2.20	1.32	1.26	0.60	0.04	0.63	0.88
	18Hb4	Fry	1.17	1.20	1.40	1.18	1.01	0.84	0.83	0.24	0.08
	19Hb1	Rf/PHI	1.01	1.93	1.94	1.25	1.24	0.64	0.01	0.54	0.98
	19Hb1	Fry	1.07	1.53	1.63	1.20	1.30	0.74	0.12	0.38	0.74
Hb20	19Hb3	Rf/PHI	1.01	1.95	1.96	1.26	1.25	0.64	0.01	0.55	0.98
	19Hb3	Fry	1.14	1.40	1.60	1.22	1.07	0.76	0.36	0.34	0.43
	19Hb5	Rf/PHI	1.04	1.91	1.99	1.28	1.22	0.64	0.05	0.55	0.88
	19Hb5	Fry	1.18	1.30	1.53	1.22	1.03	0.80	0.59	0.30	0.23
Hb22	20Hb1	Rf/PHI	1.02	1.90	1.94	1.26	1.23	0.65	0.03	0.53	0.93
	20Hb1	Fry	1.20	1.33	1.60	1.24	1.03	0.78	0.62	0.34	0.21
	20Hb2	Rf/PHI	1.06	1.82	1.93	1.27	1.20	0.66	0.07	0.52	0.82
	20Hb2	Fry	2.24	1.40	3.14	1.92	0.86	0.61	3.10	0.83	-0.41
Hb24	22Hb1	Rf/PHI	1.03	2.16	2.23	1.32	1.28	0.59	0.03	0.64	0.92
	22Hb1	Fry	1.10	1.91	2.10	1.32	1.20	0.63	0.11	0.57	0.74
	22Hb2	Rf/PHI	1.11	1.90	2.11	1.33	1.20	0.63	0.12	0.57	0.72
	22Hb2	Fry	1.06	1.27	1.34	1.12	1.06	0.84	0.20	0.22	0.63
Hb26	24Hb1	Rf/PHI	1.23	1.81	2.22	1.40	1.14	0.63	0.28	0.59	0.49
	24Hb1	Fry	1.31	1.60	2.10	1.40	1.07	0.67	0.52	0.53	0.27
	24Hb3	Rf/PHI	1.04	1.87	1.94	1.26	1.22	0.65	0.04	0.53	0.89
	24Hb3	Fry	1.23	1.30	1.60	1.25	1.02	0.78	0.77	0.33	0.12
Hb26	24Hb5	Rf/PHI	1.10	2.10	2.30	1.36	1.24	0.59	0.09	0.65	0.78
	24Hb5	Fry	1.46	1.10	1.61	1.33	0.91	0.83	4.64	0.36	-0.60
26Hb1	Rf/PHI	1.01	1.94	1.96	1.26	1.24	0.64	0.01	0.55	0.97	

Table 1 (continued)

Sample No.	Method	Rxy	Ryz	Rzx	Stretch			Principal strain Ratios K	Strain magnitude Et	lode's parameter	
					Sx	Sy	Sz				
	26Hb1	Fry	1.29	1.40	1.80	1.32	1.03	0.73	0.71	0.42	0.15
	26Hb3	Rf/PHI	1.04	2.04	2.12	1.30	1.25	0.61	0.04	0.60	0.90
	26Hb3	Fry	1.62	1.42	2.30	1.55	0.96	0.67	1.48	0.59	-0.16
	26Hb5	Rf/PHI	1.01	2.01	2.02	1.27	1.26	0.63	0.01	0.57	0.98
	26Hb5	Fry	1.08	2.12	2.30	1.36	1.25	0.59	0.08	0.65	0.80
Hb27	27Hb1	Rf/PHI	1.09	1.85	2.02	1.30	1.19	0.64	0.11	0.54	0.75
	27Hb1	Fry	1.83	2.20	4.02	1.94	1.06	0.48	0.69	0.99	0.13
	27Hb4	Rf/PHI	1.10	2.00	2.20	1.34	1.22	0.61	0.10	0.61	0.76
	27Hb4	Fry	1.06	2.36	2.51	1.39	1.30	0.55	0.05	0.73	0.87
	27Hb5	Rf/PHI	1.08	2.00	2.16	1.33	1.23	0.61	0.08	0.60	0.80
	27Hb5	Fry	1.05	1.43	1.50	1.16	1.11	0.77	0.11	0.31	0.78
Hb28	28Hb1	Rf/PHI	1.01	2.02	2.04	1.27	1.26	0.62	0.01	0.58	0.97
	28Hb1	Fry	3.51	1.31	4.60	2.53	0.72	0.55	8.03	1.15	-0.64
	28Hb4	Rf/PHI	1.03	1.90	1.96	1.26	1.23	0.65	0.04	0.54	0.91
	28Hb4	Fry	1.29	2.32	2.99	1.57	1.22	0.52	0.22	0.81	0.54
Hb29	29Hb1	Rf/PHI	1.03	2.04	2.10	1.29	1.26	0.62	0.03	0.59	0.92
	29Hb1	Fry	1.08	1.49	1.61	1.20	1.11	0.75	0.16	0.36	0.68
	29Hb4	Rf/PHI	1.02	1.90	1.94	1.25	1.23	0.65	0.02	0.53	0.95
	29Hb4	Fry	1.23	1.61	1.98	1.34	1.09	0.68	0.37	0.49	0.40
Hb31	31Hb1	Rf/PHI	1.01	1.88	1.90	1.24	1.23	0.65	0.01	0.52	0.97
	31Hb1	Fry	1.76	1.60	2.81	1.70	0.97	0.61	1.26	0.73	-0.09
	31Hb2	Rf/PHI	1.01	1.96	1.98	1.26	1.25	0.64	0.01	0.56	0.98
	31Hb2	Fry	1.00	1.41	1.42	1.12	1.12	0.79	0.00	0.28	0.99
Hb32	32Hb1	Rf/PHI	1.10	1.91	2.10	1.32	1.20	0.63	0.11	0.57	0.74
	32Hb1	Fry	1.64	1.17	1.91	1.46	0.89	0.77	3.88	0.48	-0.53
	32Hb3	Rf/PHI	1.00	1.98	1.99	1.26	1.26	0.63	0.00	0.56	0.99
	32Hb3	Fry	1.24	1.45	1.80	1.31	1.05	0.73	0.54	0.42	0.26
Hb33	33Hb1	Rf/PHI	1.13	1.87	2.11	1.34	1.18	0.63	0.15	0.57	0.67
	33Hb1	Fry	1.15	1.41	1.62	1.23	1.07	0.76	0.36	0.35	0.42
Hb35	35Hb3	Rf/PHI	1.05	1.72	1.80	1.23	1.18	0.69	0.06	0.46	0.85
	35Hb3	Fry	1.78	1.20	2.14	1.56	0.88	0.73	3.81	0.56	-0.51
	35Hb5	Rf/PHI	1.08	1.71	1.85	1.26	1.16	0.68	0.12	0.47	0.74
	35Hb5	Fry	1.58	1.20	1.90	1.44	0.91	0.76	2.92	0.47	-0.43
Hb36	36Hb1	Rf/PHI	1.04	1.90	1.98	1.27	1.22	0.64	0.04	0.54	0.89
	36Hb1	Fry	1.09	1.50	1.64	1.21	1.11	0.74	0.19	0.37	0.64
	36Hb2	Rf/PHI	1.16	1.90	2.20	1.37	1.18	0.62	0.18	0.59	0.63
	36Hb2	Fry	1.69	1.24	2.10	1.53	0.90	0.73	2.86	0.54	-0.42
Hb37	37Hb1	Rf/PHI	1.07	1.80	1.93	1.28	1.19	0.66	0.09	0.51	0.78
	37Hb1	Fry	1.08	1.02	1.10	1.06	0.98	0.96	3.92	0.07	-0.58
	37Hb3	Rf/PHI	1.08	1.80	1.94	1.28	1.19	0.66	0.10	0.51	0.77
	37Hb3	Fry	1.43	1.75	2.50	1.53	1.07	0.61	0.57	0.65	0.22
	37Hb4	Rf/PHI	1.11	1.90	2.10	1.32	1.20	0.63	0.12	0.57	0.73
	37Hb4	Fry	1.03	1.35	1.40	1.13	1.09	0.81	0.10	0.26	0.80
Hb38	38Hb1	Rf/PHI	1.02	1.66	1.70	1.20	1.17	0.71	0.04	0.42	0.91
	38Hb1	Fry	1.41	1.40	1.97	1.40	1.00	0.71	1.02	0.48	-0.01
	38Hb2	Rf/PHI	1.11	1.62	1.80	1.26	1.13	0.70	0.18	0.44	0.64
	38Hb2	Fry	1.12	1.52	1.70	1.24	1.11	0.73	0.23	0.40	0.58
	38Hb5	Rf/PHI	1.13	1.70	1.92	1.29	1.15	0.67	0.18	0.49	0.63
	38Hb5	Fry	1.32	2.04	2.70	1.53	1.16	0.57	0.31	0.72	0.44

generated during the epizonal metamorphism are concordant with the foliation. Major structures related to this first phase are scarcely distinguishable in the field; they can be kilometer-size folds with, according to detailed structural data, a roughly vertical axial-plane schistosity (S1) striking north–south.

The second phase of folding, which typically deforms the metamorphic foliation (S1), is well expressed through various scales of observation. In the area 10 km southeast of Sanam, aerial photomicrographs disclose folds of several kilometers which, according to field data, are a succession of overturned antiforms and synforms. These large structures are accompanied by parasitic cylindrical and asymmetric isoclinal folds of between a few meters to a few centimeters in size in the greywacke beds. Interbedded pelitic facies are microfolded (millimeter size): in thin section, the minor folds are seen to

be related to axial plane strain-slip cleavage (Sz) and often to microlithons, still bearing metamorphic minerals such as chlorite and sericite.

The third phase of deformation, which was induced by doming effects, is represented by metric undulations of the metamorphic foliation (S1) or the second-phase fold axes. There is also a corresponding jointing or rough axial-plane schistosity (S3), which is generally oriented N 60° E and vertical. Although it is the last folding observed in the Lanit-Urdsynclorium the dispersion of the poles of schistosity (S3) and of lineation (L3) suggests that there was a later deformation.

This work shows that the Rf/ ϕ related strains analysis resulted from semi brittle to ductile-deformed feldspar and mafic minerals related to thrusting inspired deformation.

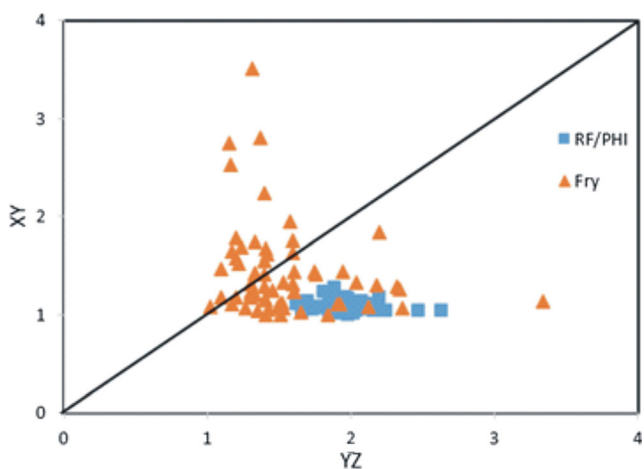


Fig. 6 : Flinn plot shows strain symmetry from obtained data for R_f/ϕ (Blue Square) and Fry (orange Triangle) methods (Flinn 1962)

These data indicates the time of deformation represents the accumulation of deformation during thrusting and intrusions. The microstructure of the area is dominantly characterized by pervasive and subhorizontal foliations from the main

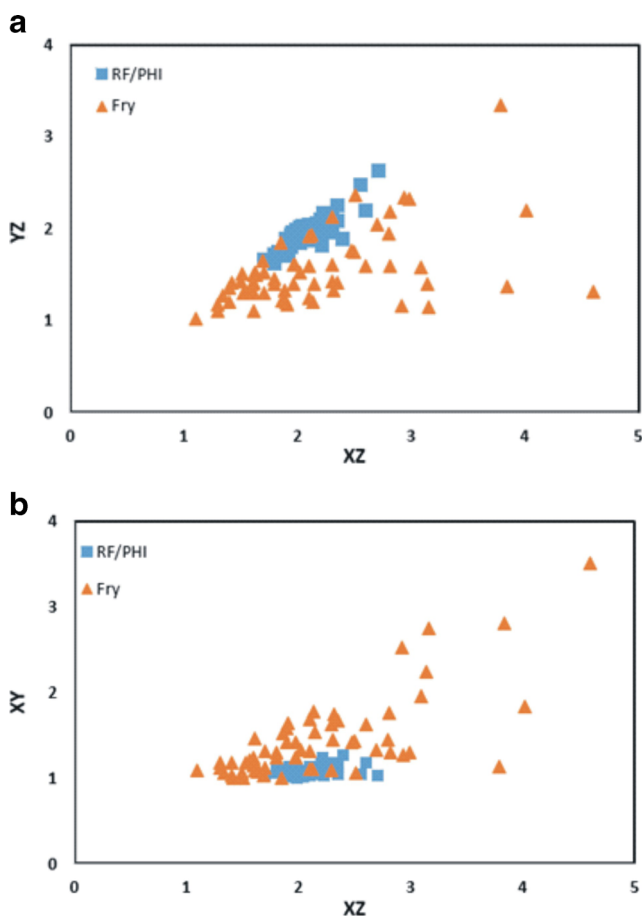


Fig. 7 a) The ratio between XZ vs YZ shows positive correlation for R_f/ϕ (Blue Square) and Fry (orange Triangle) methods. b) The ratio between XZ vs XY shows more or less constant for R_f/ϕ (blue square) and Fry (orange triangle) method

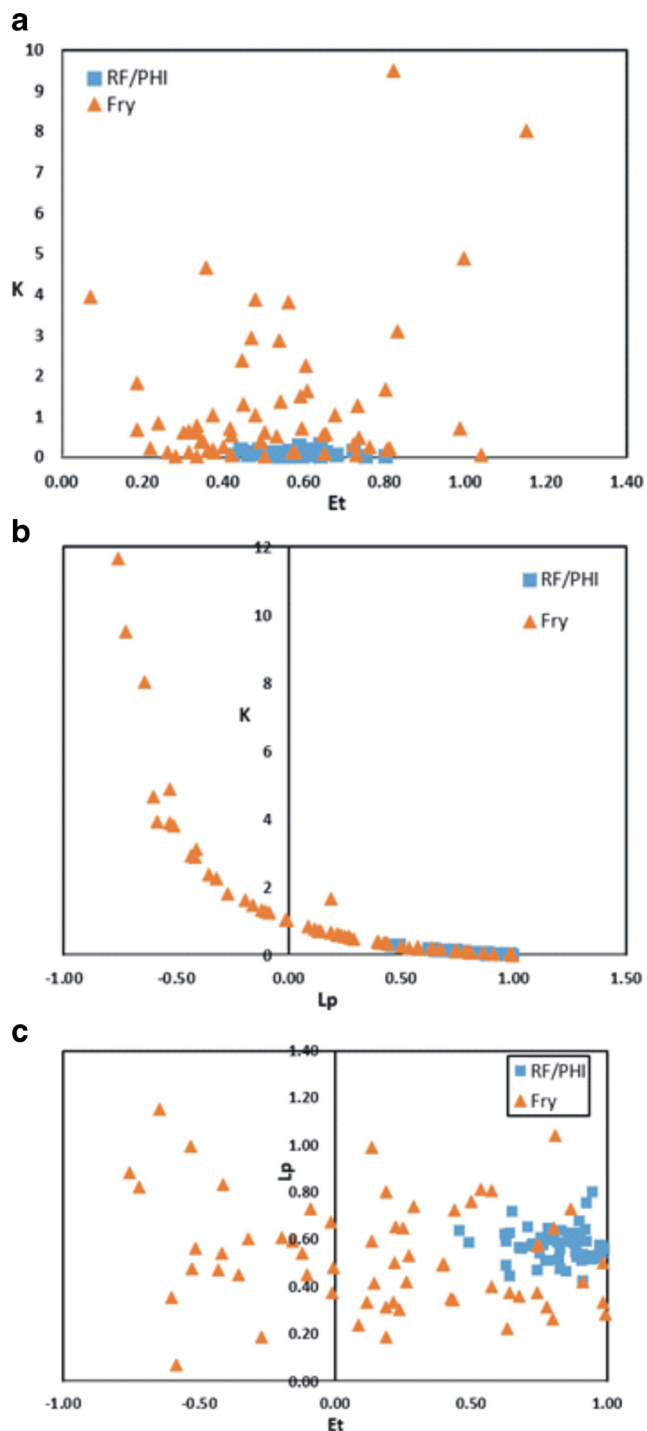


Fig. 8 a) The relationship between ET vs K shows the obtained data for R_f/ϕ (Blue Square) less than Fry method (orange triangle). b) The relationship between LP vs K showing negative correlation for the strain data, R_f/ϕ (Blue square) and Fry (orange triangle) method. c) The ratio between LP vs ET shows the obtained data for R_f/ϕ (Blue square) and for Fry (orange triangle) methods mainly constant

metamorphic phase, which are almost subparallel to the fault contacts in the Halaban area.

Kassem and Ring (2004) have reported that only minor or lack of volume changes can be expected in the high-grade

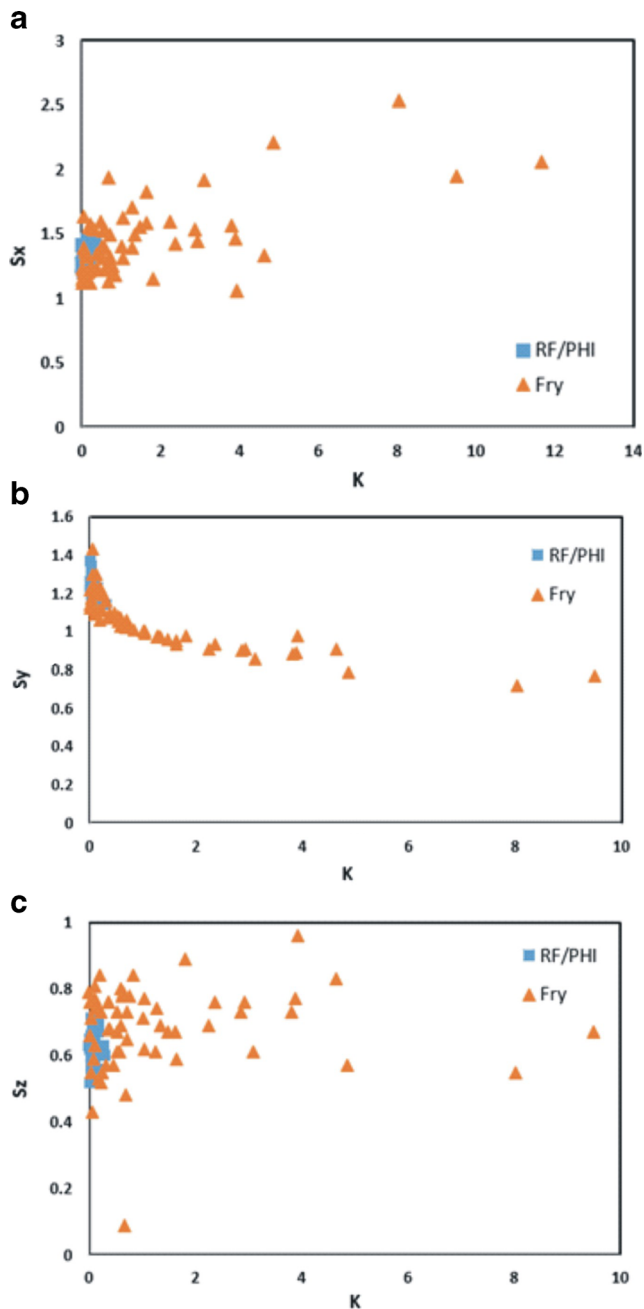


Fig. 9 a) The ratio between X axis (SX) vs strain symmetry (K) shows a positive correlation for the R_f/ϕ (Blue square) and Fry methods (orange triangle). b) The average between Y axes (SY) vs strain symmetry (K) shows a negative correlation for the R_f/ϕ (Blue square) and Fry methods (orange triangle). c) The average between Z axis (SZ) vs strain symmetry (K) shows a no obvious correlation for the R_f/ϕ (Blue square) and Fry methods (orange triangle)

metamorphic rocks if their porosities remain very low during deformation. The finite strain data dominantly show oblate strain and prolate strain symmetry in the studied Ar-Halaban area. This indicates that the accumulation of ductile deformation during thrusting was not only caused by simple shearing but a vertical shortening also played its role by pure

shearing. Vertical shortening caused the subhorizontal foliation in the Halaban area.

Conclusions

The results of finite strain data from Halaban area are summarized as follows:

- The Halaban area is controlled by thrust faults in eastern Arabian Shield.
- The strain ellipsoids in the Halaban area were affected by oblate strain symmetry and some data show prolate strain symmetry.
- R_f/ϕ and Fry methods show that no difference in the deformation behavior in the studied area,
- The different types of rocks in the Halaban area displayed the same order of magnitude and deformation.
- The obtained of finite strain data concluded that the Halaban area resulted from simple-shear deformation.

Acknowledgements This project was supported by King Saud University, Deanship of Scientific Research, College of Science Research Center.

References

- Al-Saleh AM, Kassem OM (2012) Microstructural finite strain analysis and $40\text{Ar}/39\text{Ar}$ evidence for the origin of the Mizil gneiss dome, eastern Arabian shield, Saudi Arabia. *J Afr Earth Sci* 70:24–35
- Al-Saleh AM, Boyle AP (2001) Neoproterozoic ensialic back-arc spreading in the eastern Arabian shield: geochemical evidence from the Halaban ophiolite. *J Afr Earth Sci* 33:1–15
- Al-Saleh AM, Boyle AP, Mussett AE (1998) Metamorphism and $40\text{Ar}/39\text{Ar}$ dating of the Halaban ophiolite and associated units: evidence for a two-stage orogenes in the eastern Arabian shield. *Journal Geological Society London* 155:165–175
- Al-Shanti AM, El-Mahdy OR (1988) Geological Studies and Assessment of Chromite Occurrences in Saudi Arabia. KACST Project No. AT-6-094
- Al-Shanti AMS, Mitchell AHG (1976) Late Precambrian subduction and collision in the Al Amar-Idhas region. *Arabian shield, Kingdom of Saudi Arabia: Tectonophysics* 30:T41–T47
- Al-Shanti HA, Abo Omar JM (2003) Effect of olive cake on layers' performance and egg quality. *Journal Al-Azhar University, Gaza (Natural sciences)*, 6 (1)
- Camp VE (1984) Island arcs and their role in the evolution of the western Arabian shield. *Geol Soc Am Bull* 95:913–921
- Delfour J, (1979) Geologic Map of the Halaban quadrangle, sheet 23G, Kingdom of Saudi Arabia Deputy Ministry for Mineral Resources Geoscience Map GM 46C, scale 1:250 000, with text, 32 p
- Delfour J, (1981) Geologic map of the Al Hissu quadrangle, sheet 24 E, Kingdom of Saudi Arabia: Saudi Arabian Deputy Ministry for Mineral Resources Geologic Map GM-58, 47 p
- Doeblich JL, Al-Jehani AM, Siddiqui AA, Hayes TS, Saleh Y, Wooden JL, Johnson PR, Kattan FH, Shaikan B, Basahel M, Zahran H, Al-Shammari A (2007) Geology and mineral resources of the Ar Rayn

- terrane. Eastern Arabian Shield, Kingdom of Saudi Arabia, Precambrian Research 158:17–50
- Flinn D (1962) On folding during three-dimensional progressive deformation. *Quarterly Journal of Geological Society of London* 118:385–433
- Fry N (1979) Random point distributions and strain measurement in rocks. *Tectonophysics* 60:89–105
- Garson MS, Shalaby IM (1976) Precambrian–lower Paleozoic plate tectonics and metallogenesis in the Red Sea region. *Geol. Assoc. can. Spec Pap* 14:573–596
- Gass IG (1977) The evolution of the pan-African crystalline basement in NE Africa and Arabia. *J Geol Soc Lond* 134:129–138
- Hossack, J R (1968) Pebble deformation and thrusting in the Bygdin area Southern Norway, *Tectonophysics* 5:315–339
- Johnson PR, Andresen A, Collins AS, Fowler AR, Fritz H, Ghebreab W, Kusky T, Stern RJ (2011) Late Cryogenian–Ediacaran history of the Arabian–Nubian shield: a review of depositional, plutonic, structural, and tectonic events in the closing stages of the northern east African Orogen. *J Afr Earth Sci* 61:167–232
- Kassem OMK, Abd El Rahim SH, El Nashar ER (2012) Strain analysis and microstructural evolution characteristic of Neoproterozoic rocks associations of Wadi el Falek, Centre Eastern Desert, Egypt. *Geotectonics*, 46. No. 5:379–388
- Kassem OMK (2015) Investigation of kinematic analysis in the Tanumah area, Arabian shield, Saudi Arabia. *Journal of Tethys* 3(1):16–30
- Kassem OMK, Hamimi Z (2014) Application of finite strain technique for deformed lithologies in Al Amar suture, eastern Arabian shield. *The Open Geology Journal* 8(Suppl 1: M7):97–106
- Kassem OMK (2011) Determining heterogeneous deformation for granitic rocks in the northern thrust in Wadi Mubark belt, Eastern Desert, Egypt. *Geotectonics journal*. 45. No 3:244–254
- Kassem OMK (2014) Kinematic analysis of the Migif area in the Eastern Desert of Egypt. *J Afr Earth Sci* 90:136–149
- Kassem OMK, Abdel Raheim S (2010) Finite strain analysis for the metavolcanic-sedimentary rocks in the Gabel el- Mayet region, central Eastern Desert, Egypt. *J Afr Earth Sci* 58:321–330
- Kassem OMK, Ring U (2004) Under plating-related finite-strain patterns in the gran Paradiso massif, western alps, Italy: heterogeneous ductile strain superimposed on a nappe stack. *J Geol Soc Lond* 161: 875–884
- Kemp J, Gros Y, Prian J-P (1982) Geologic map of the Mahd adh Dhahab quadrangle sheet 23E, Kingdom of Saudi Arabia: Saudi Arabian Deputy Ministry for Mineral Resources Geologic Map GM-64, scale 1: 250,000, 39 p
- Nehlig P, Genna A, Asfirane F (2002) A review of the pan-African evolution of the Arabian shield. *GeoArabia* 7:103–124
- Passchier CW, Trouw RA (1995) *Microtectonics*. Springer, Berlin Heidelberg New York, 366 pp
- Ramsay JG (1967) *Folding and fracturing of rocks*. McGraw-Hill, New York, London, 568 pp
- Ramsay JG, Huber M (1983) *The techniques of modern structural geology, volume 1, strain analysis*. Academic Press, London
- Ring U (1998) Exhumation of blue schists from Samos Island. *Geological Society of Greece Bulletin* V. 32, pp. 97–104. Saudi Arabia. *J Geol Soc Lond* 136:441–454
- Schmidt DL, Hadley DG, Stoesser DB (1979) Late Proterozoic crustal history of the Arabian shield southern Najd province. Kingdom of Saudi Arabia: King Abdulaziz University Institute of Applied Geology Bulletin 3(2):41–58
- Stoesser DB, Stacey JS, Greenwood WR, Fischer LB (1984) U/Pb Zircon Geochronology of the Southern Part of the Nabitah Mobile Belt and Pan-African Continental Collision in the Saudi Arabian Shield”, Saudi Arabian Deputy Ministry for Mineral Resources Technical Record USGS-TR-04-5, pp. 88
- Stoesser DB (1986) Distribution and tectonic setting of plutonic rocks of the Arabian shield. *Journal African Earth Sciences* 4:21–46
- Stoesser DB, Camp VE (1985) Pan-African microplate accretion of the Arabian shield. *Geol Soc Am Bull* 96:817–826
- Vail JR (1983) Pan-African crustal accretion in Northeast Africa. *J Afr Earth Sci* 1:285–294